

Summary. — Granular media such as sand and sugar are ubiquitous in nature and industry but are less well understood than fluids or solids. We consider the behavior of rapid granular flows where the transfer of momenta by collisions dominates. The physics is quite different for the opposite limit of static or slowly moving grains (e.g., sand piles). To gain understanding of granular flows we consider two problems that have been investigated with experiments, particle simulations and hydrodynamic theory: vertically oscillating granular layers and flow past an obstacle. Oscillating granular layers spontaneously form spatial patterns when the container acceleration amplitude exceeds a critical value, about 2.5 times the gravitational acceleration. Simulations with hard spheres that conserve linear momentum and dissipate energy in collisions are in qualitative accord with some but not all aspects of the observed patterns. It is necessary to include friction and angular momentum conservation in the simulations to achieve quantitative accord with observations.

The applicability of a hydrodynamic theory to granular flows is not obvious because for typical conditions the particle mean free path is comparable to the length scale over which velocity and density fields change; hence there is not the separation of scales needed to justify a hydrodynamic approach. However, we show that Navier-Stokes-like equations describe well the density and temperature fields in vertically oscillating layers, even though this system is far from isothermal, incompressible fluid dynamics.

The second problem examined, flow past an obstacle, is also described well by particle simulations for frictional dissipative particles, but continuum simulations are only in qualitative accord with the observations. We show that continuum theory fails because it does not include friction between particles. Finally, we discuss how shock waves are common in granular flows since the the speed of sound (pressure waves) in a granular gas is typically only a few centimeters/second, while mean flow speeds are typically meters/second. Comparison of shocks in granular experiments and simulations is made with shocks in ordinary gases. Much more research is needed to understand how shocks evolve in granular flows.

Pattern formation and shocks in granular gases

To appear in Proceedings of The International School of Physics Enrico Fermi Course CLV "The Physics of Complex Systems (new advances and perspectives)" edited by F. Mallamace and H. E. Stanley (IOS Press, Amsterdam, 2004).

HARRY L. SWINNEY, E.C. RERICHA

Center for Nonlinear Dynamics and Department of Physics, University of Texas at Austin, Austin, Texas 78712 USA

1. – Introduction

Granular materials include sand, sugar, crushed coal, cereals, pills, cosmetics, and asteroids. The transport, mixing, and segregation of granular materials is important in the pharmaceutical, mining, agricultural, metal, food, and energy industries. Even in the chemical industry, the majority of the products are in granular rather than liquid form [1]. Thus a large engineering literature has developed on "powders and particulates". However, a basic understanding of the physical mechanisms underlying the collective behavior of particles in a granular medium is lacking. Granular media can exhibit both solid and fluid properties (e.g., one can walk on a beach or pour the sand from a bucket), but granular media are less well understood than solids and fluids. While fluids are processed in industry with high efficiency, the efficiency of handling (crushing, mixing, separation) of granular materials is estimated to be well below optimum [1].

The scientific study of granular systems has a long history, including a discussion by Galileo in his *Dialogues* and an 1831 study by Faraday of convective motion of grains in heaps in vertically oscillated granular layers [2]. In recent years there has been a resurgence of interest in granular media among physicists, thanks to Pierre-Giles de

Gennes, who recommended in the early 1980s to young French scientists that granular matter was an interesting subject worthy of study [3-6]. In the past two decades there has been an explosion of interest in granular systems. A search in INSPEC on the word “granular” followed by “system, medium, matter, flow, or gas” yields 20 papers in the three year period 1980-82, while a decade later the number of papers in a three year period jumped to 112, and in 2000-2002 there were 691 papers on the subject. The growth is not so dramatic for literature searches using terms often used in industry (powder, particles, particulates), but most of that work is empirical, and much of that literature concerns pastes, soil, and fine particles (powders). We make no attempt to review the enormous literature on granular/particulate matter but list a few reviews [7-13], books [14-18], and several journals: *Powder Technology*, *Granular Matter*, *Particle Science and Technology*, and *Advanced Powder Technology*.

The key property distinguishing collisions of granular particles from collisions of atoms in an ordinary gas is dissipation: collisions between macroscopic grains are inelastic – in the absence of external forcing, the particles in a granular medium all come to rest. A measure of this dissipation is the coefficient of restitution e , which is the ratio of the relative normal velocity of two particles after a collision to the relative normal velocity before collision. Some representative values of e for a relative normal velocity of 0.1 m/s are 0.96 for hardened bronze, 0.85 for aluminum, and 0.3 for lead [19]; the values depend on the particle bulk and surface properties in a complicated way (see, e.g., [20]).

This chapter concerns rapid granular flows, which is called the collisional regime to distinguish it from the quasi-static regime where particles are at rest or nearly so. Much of the granular literature concerns the quasi-static regime where inertia is not significant and chains of particles in contact bear most of the load. Understanding the development and evolution of these force chains and the role of steric hindrance is often the focus of the research on sand piles and other granular systems at rest or nearly at rest. The collisional and quasi-static regimes are each difficult, but the intermediate regime with some particles moving rapidly while others are at rest is even more difficult. For an example, see the contribution in this book on the formation of craters in a granular medium [21, 22].

We will consider situations where only contact forces are important. For small particles (less than $\approx 50 \mu\text{m}$), electrostatic and van der Waals forces become important. Further, air friction can be significant, but for particles greater than about 1 mm in diameter, air friction is often negligible if the velocity is not too large.

An oft-studied example of a granular medium in the collisional regime is a collection of particles in a vertically oscillating container. Section 2 describes spatial patterns formed by such a system. Since the number of particles in an experiment can be small (less than one million), Newton’s laws for the motion of these particles can be directly implemented on a Personal Computer. Section 3 discusses such Molecular Dynamics (MD) simulations for hard, spherical particles that are characterized by a restitution coefficient and a frictional coefficient. Most theoretical analyses of granular flows examine frictionless (smooth) inelastic spheres, but there exist no frictionless macroscopic particles, just as there are no elastic particles. Molecular dynamics simulations show that realistic

models of rapid granular motions must include friction – friction provides another mode of dissipation and also results in reduced grain mobility and a higher particle collision rate [23]. Molecular dynamics simulations including friction describe experimental observations on oscillating granular media very well, as we shall describe in Section 3, but simulations without friction fail to capture even qualitatively some important aspects of the observations.

Studies of oscillated granular layers have revealed localized structures, “oscillons”, which are stable for a range of container oscillation frequencies and amplitudes. Section 4 describes the properties of oscillons and shows how they can be considered as the basic building blocks of some extended spatial patterns.

The continuum approach to granular flows is introduced in Section 5, where equations of motion derived by Jenkins and Richman for a dilute dissipative fluid are presented. The Jenkins-Richman equations are similar to the Navier-Stokes equations for a fluid but are modified to include dissipative effects arising from collisions between the grains. However, the equations do not include the effect of friction in grain-grain collisions or grain-container collisions. As will be discussed, the application of continuum equations to granular flows must be considered with caution because, unlike an ordinary fluid, in granular flows there is not a large separation between the microscopic and macroscopic length and time scales.

In a granular fluid the speed of propagation of pressure fluctuations (the sound speed) is only a few centimeters/sec, which is very small compared to the 330 m/s sound speed in air. (The granular sound speed here refers to particles in vacuum; there is no air and the only particles are the dissipative grains.) Hence the average streaming speed of granular flows generally exceeds the sound speed in the flow, and shock waves form whenever the flow encounters an obstacle. These shock waves are the subject of Section 6, where observations from experiments are compared with molecular dynamics and continuum simulations.

We will conclude with a discussion in Section 7 that mentions some of the many issues open in the understanding of systems of dissipative particles.

2. – Patterns in vertically oscillated granular layers

Consider a layer of non-cohesive grains in a container oscillating sinusoidally with frequency f and dimensionless acceleration amplitude $\Gamma = 4\pi^2 f^2 A/g$, where $2A$ is the peak-to-peak amplitude of the displacement of the container and g is the gravitational acceleration. We consider patterns that arise spontaneously, not from sidewall forcing or from interstitial gas, but from correlations induced by multiple collisions between the grains and between the grains and the container bottom. To minimize sidewall effects, the horizontal dimensions of the container are made large compared to the layer depth h . The layer is illuminated from the side, as fig. 1 illustrates [24, 25].

For $\Gamma > 1$, on each cycle the layer loses contact with the container, flies in the air, and then collides with the container. However, the layer remains compact and flat until $\Gamma \approx 2.5$, where a standing wave pattern spontaneously forms. A square pattern forms at

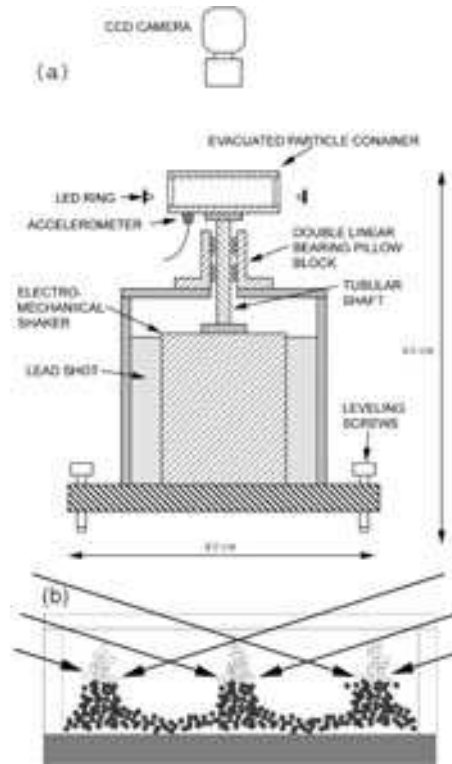


Fig. 1. – (a) Electromechanical shaker system for studying pattern formation in vertically oscillating layers. (b) Spatial patterns are illuminated from the side by light incident at low angles. When viewed from above, high regions are bright and low regions are dark. From [24].

low frequencies and a stripe pattern at high frequencies, as figs. 2(a) and (b) respectively illustrate [26, 27]. The pattern is subharmonic, repeating every 2τ , where $\tau = 1/f$ is the container oscillation period; thus a ridge in a striped pattern at an instant of time becomes a valley one container oscillation period later.

A heuristic argument for the critical value of Γ for the onset of instability of a flat oscillating layer was given in [25]. The authors argued that a flat layer becomes unstable when the collision occurs at the plate's lowest point. Then a time $\tau/2$ is taken for the layer to free fall from its highest point through a distance $2A$ to collide with the plate, so that $2A = \frac{1}{2}g(\tau/2)^2 = \frac{1}{8}g\tau^2$, which gives $\Gamma_c = 2.5$, in accord with the observed critical acceleration for the onset of patterns.

The onset of patterns (squares or stripes) at $\Gamma \approx 2.5$ is quite robust, independent of layer depth (depths from about a monolayer to about 25 particle diameters σ), container shape, and particle properties (size, restitution coefficient, surface roughness, material). Most studies of patterns have been conducted for particles of uniform size, but studies

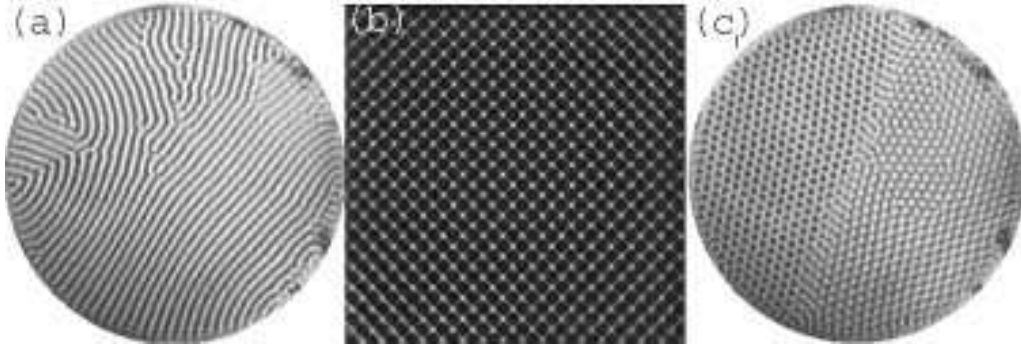


Fig. 2. – Patterns in oscillating granular layers: (a) stripes, (b) squares, and (c) hexagons (with different phases on the left and right). The patterns oscillate at $f/2$, where f is the container oscillation frequency. Here Γ , f , and h/σ (ratio of the depth of the layer at rest to the diameter of the particles) are given by (a) 3.3, 67 Hz, 7, (b) 2.9, 25 Hz, 4, and (c) and (d) 4.0, 67 Hz, 7. In (a) and (c) the diameter of the container is 770σ and in (b) the container is square, $1100\sigma \times 1100\sigma$. The particles are bronze spheres 0.165 mm diameter. (a) and (c) are from [26] and (b) is from [27].

with a range of particle sizes have found that the onset remains sharp for size distributions ranging up to about 30% [28]. Square and stripe patterns have also been observed to form at $\Gamma \approx 2.5$ for irregular particles such as rice grains and grass seed [28].

The phase diagram (fig. 3) shows the stability regions for different patterns as a function of Γ and dimensionless frequency f^* , where $f^* = \sqrt{h/g}$ and h is the depth of the layer at rest [29]. The transitions are well defined and are only weakly dependent on f^* . Except for the transition from a flat layer to squares, the hysteresis is small or perhaps zero. We know of no argument for the square to stripe transition as a function of frequency with Γ fixed, but we note that the transition has been found to occur at $f^* \approx 1/3$ [24].

Some insight into the dynamics can be gained from consideration of the one-dimensional motion of a single completely inelastic ball on a vertically oscillating plate [30]. Such a model cannot of course describe the 2D spatial patterns that form in granular layers on an oscillating plate, but it does help in understanding the transitions in behavior as a function of Γ [26, 29]. The inelastic ball motion, illustrated in fig. 4, models the center of mass motion of a granular layer at small Γ , where the layer remains fairly compact and is highly dissipative as a consequence of multiple collisions. We will refer to the inelastic ball as “the layer”, meaning the motion of the center of mass of the granular layer.

For $\Gamma > 1$, the layer leaves the plate at the point in each cycle when the plate acceleration exceeds $-g$. The layer continues in free flight until it later collides with the plate. In the regime with squares or stripes oscillating at $f/2$, the layer leaves and hits the plate every cycle, as fig. 4(a) illustrates. At $\Gamma \approx 4.0$, there is a bifurcation in the dynamics, illustrated by fig. 4(b): successive trajectories now have different flight

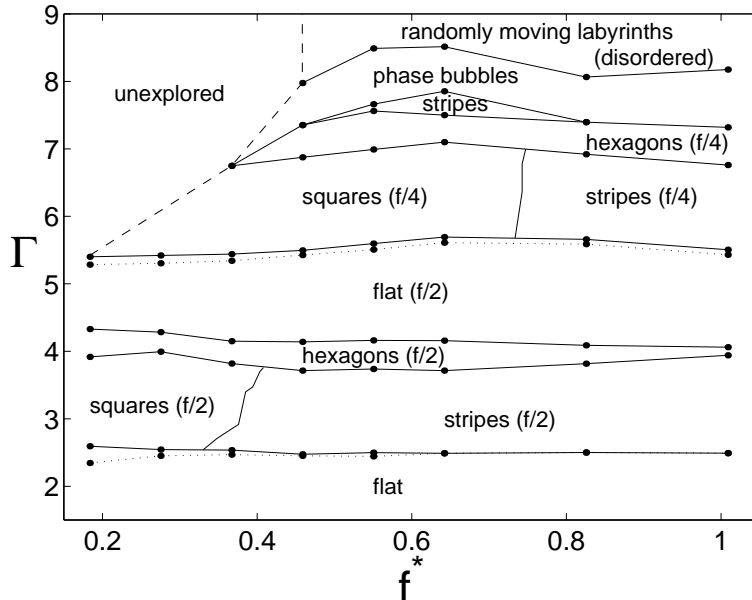


Fig. 3. – Phase diagram for granular patterns observed in a vertically oscillated container, as a function of the dimensionless acceleration Γ and dimensionless frequency $f^* = f\sqrt{h/g}$. The transitions from a flat layer to squares are hysteretic: solid lines denote the transition for increasing Γ while dotted lines denote decreasing Γ . (Bronze spheres, $\sigma = 0.165$ mm; layer depth, 5.0σ ; container diameter, 770σ .) From [29].

urations, with a short trajectory initiated by a collision of the layer with the plate whose acceleration greater than g , followed by a long trajectory initiated by a collision of the layer with the plate whose acceleration is less than g . This bifurcation corresponds to a value of Γ close to that for the onset of hexagonal spatial patterns [26], pictured in fig. 2(c). While square or stripe patterns have the same appearance whether an image is obtained at a time t or $t + \tau$, hexagonal patterns at these two times are different. The two phases are both present and are separated by a phase discontinuity in fig. 2(c) – the pattern on the right consists of a hexagonal array of dots, while the hexagonal pattern on the left is cellular; the two patterns will be switched one period, τ , later.

Another bifurcation in the dynamics occurs for $\Gamma > 4.5$, where the layer flight duration exceeds τ , and the layer hits the container every other cycle. Now the velocity of the layer relative to the plate at the instant of collision goes to zero (at about $\Gamma = 4.6$), and the layer makes a soft landing; not enough momentum is transferred from the vertical to horizontal direction to form patterns. When Γ is increased above about 5.4, there is again a transition from a flat layer to a pattern, stripes at low frequencies and squares at high frequencies. However, now the pattern period is $f/4$ instead of $f/2$. Further increase in Γ leads to another bifurcation from trajectories with a single period to suc-

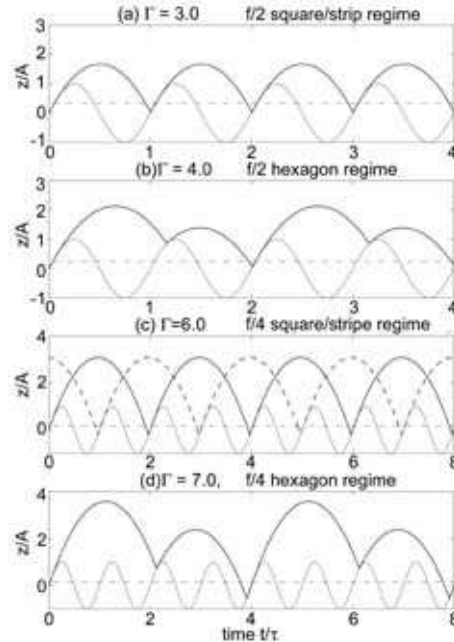


Fig. 4. – Trajectory of a completely inelastic ball on an oscillating plate. This is a model for the motion of the center of mass of a granular layer. The sinusoidal curve is the trajectory of the plate. The ball leaves the plate when the acceleration of the plate becomes $-g$, that is, when the dot-dashed line intersects the trajectory of the ball. If the ball collides with the plate above the dot-dashed line, as in (b) and (d), it leaves the plate immediately. From [29].

cessive trajectories with different flight durations (fig. 4(d)). Again this bifurcation in the dynamics of a ball corresponds to the bifurcation of the patterns from squares or stripes to hexagons.

At larger Γ the layer becomes sufficiently dilated so that the inelastic single ball model no longer provides a useful description of the dynamics. But even the $f/3$ and $f/6$ regimes of the single ball model ($8 < \Gamma < 11$) have been observed transiently in molecular dynamics simulations and laboratory experiments [29].

3. – Molecular Dynamics simulations

Simulations of granular media using rigid particles, soft particles, and Monte Carlo methods have been conducted by many researchers since the 1980s [7, 15, 31]. We consider a granular layer modeled as a collection of hard spheres that interact only through instantaneous binary collisions. Between successive collisions the particles move only under the influence of gravity. This is known as an Event Driven (ED) type of Molecular Dynamics (MD) simulation [32]. Linear and angular momentum are conserved in colli-

sions, while energy is dissipated through collisions and surface friction. The interaction between particles is described by the coefficient of restitution e , the coefficient of sliding friction μ , and the rotation coefficient of restitution β . (The same values of e , μ and β are used for ball-wall collisions as for ball-ball collisions.) This collision model was developed by Walton [33] and used in hard sphere MD simulations conducted by Bizon [25] and Moon [29], as we shall describe.

The restitution coefficient is often taken to be a constant in MD simulations, but a constant value of e can lead to “inelastic collapse”, where particles undergo an infinite number of collisions in a finite amount of time [34-36]. However, physically e must approach unity as the relative normal velocity v_n approaches zero (the elastic limit). The simulations presented here assume a form for e that goes to unity in the $v_n \rightarrow 0$ limit: $e(v_n) = 1 - Bv_n^{\frac{3}{4}}$ for $v_n < v_0$, where v_0 is a crossover velocity, and $e(v_n) = e_0 = \text{constant}$ for $v_n > v_0$. The approach of e toward unity for low v_n avoids inelastic collapse, while the constant value e_0 at high v_n is computationally efficient. The MD results are insensitive to the form assumed for $e(v_n)$ for $v_n < v_0$, as long as $e(v_n)$ increases to unity as v_n approaches zero [25].

In a collision the tangential impulse is given by μ times the normal impulse, with a cutoff corresponding to the crossover from a sliding contact to a rolling contact. The crossover ratio of the relative surface velocity after collision to that before the collision is given by β , which we fix at -0.35, as in [33]. The parameters e_0 and μ are set to 0.7 and 0.5, respectively, values obtained by fitting MD simulation results to laboratory observations for square patterns in layers of lead particles at one set of conditions [25].

Results from simulation and experiment are compared in fig. 5 for seven values of (f^*, Γ) . At every point in the phase diagram in fig. 3, the results from the MD simulation agree with experiment, not only in the form of the pattern but also in the wavelength of the pattern. The dispersion relation relating the wavelength λ to f^* for layers of varying depths collapse onto a single curve, $\lambda/h = 1 + 1.1f^{*-1.32 \pm 0.03}$, when the container velocity exceeds a critical value, $v_{gm} \approx 3\sqrt{\sigma g}$, where v_{gm} corresponds to a transition in the grain mobility (gm): for $v > v_{gm}$, there is a hydrodynamic-like horizontal sloshing motion of the layer, while for $v < v_{gm}$, the grains are essentially immobile and the stripe pattern apparently arises from a bending of the granular layer [24].

Most MD simulations and theoretical analyses of granular media consider frictionless spherical particles [37-39]. However, MD simulations comparing the behavior of frictional and frictionless particles indicate that the effect of friction cannot be mimicked by increasing the dissipation (decreasing e) [23]; thus friction is not merely an additional mechanism of dissipation. Even a small amount of friction increases the overall dissipation significantly, not because the frictional dissipation is significant in each collision, but because the friction reduces the grain mobility and increases the overall collision rate. MD simulations with frictional particles yield square and hexagonal patterns like those observed in experiments (fig. 5), while simulations without friction do not yield square or hexagonal patterns, even if the restitution coefficient is decreased to compensate for the absence of friction [23]. Simulations of frictionless particles do yield stripe patterns, but the critical Γ for the onset of patterns is smaller ($\Gamma_c \approx 1.9$) than for frictional particles

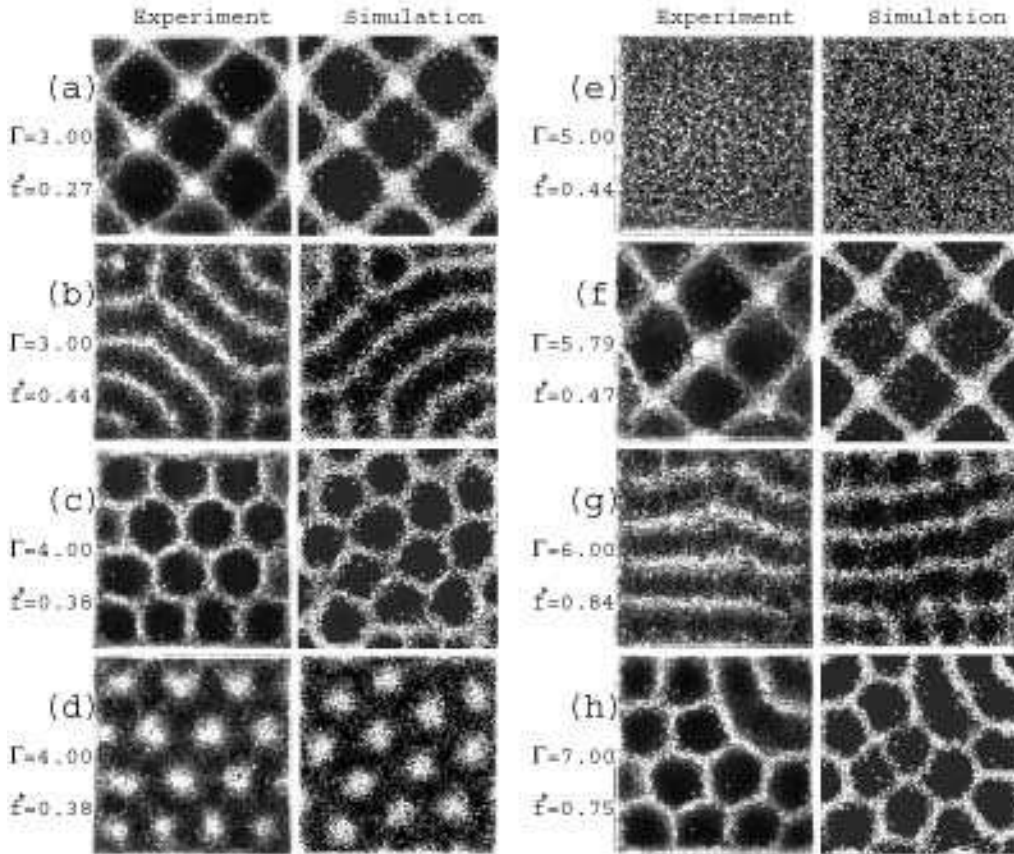


Fig. 5. – Standing wave granular patterns in laboratory experiments and molecular dynamics simulations for the same number of particles, 60,000, which fill a $100\sigma \times 100\sigma$ container to a depth of 5.4 layers: (a) squares, (b) stripes, (c) and (d) alternating phases of hexagons, (e) flat layers, (f) squares, (g) stripes, and (h) hexagons. Patterns (a)-(e) oscillate at $f/2$, (f)-(h) at $f/4$. The experiment used lead particles with $\sigma = 0.55$ mm. From [25].

($\Gamma_c \approx 2.5$), and the stripes formed by frictionless particles are less robust than those formed by particles with friction [23].

4. – Localized structures and lattice dynamics

Localized stable standing wave structures dubbed “oscillons” can occur in oscillating granular layers when Γ is decreased slightly below the value corresponding to the onset of squares with increasing Γ [28,40]. Top and side views of oscillons are shown in fig. 6. An oscillon is a small, circularly symmetric excitation that oscillates at $f/2$; during one cycle of the container, it is a peak; on the next cycle it is a crater. Unlike solitons, oscillons

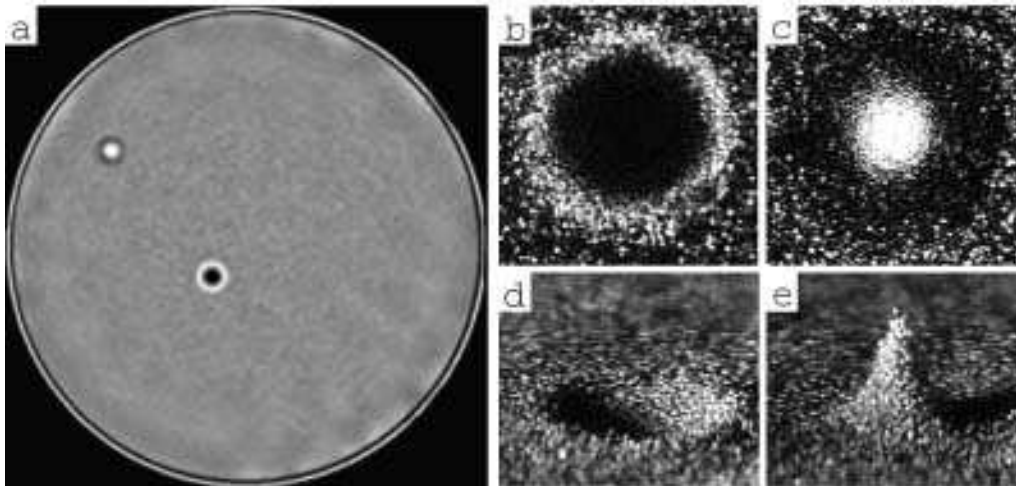


Fig. 6. – (a) Snapshot of a container with two oscillons (viewed from above); one is a peak (upper left) and the is other a crater (near the center). (b) and (d), Close-ups of an oscillon crater viewed from the top and from the side, respectively. (c) and (e) Close-ups of an oscillon peak viewed from the top and from the side, respectively. Individual bronze spheres ($\sigma = 0.165$ mm) are discernible in (b)-(e). ($f = 25$ Hz, $\Gamma = 2.45$, layer depth $h = 17\sigma$.) From [28].

are stationary (nonpropagating). Oscillons form with equal probability at all locations in the container, and they live indefinitely. If the container acceleration were increased slowly from rest to a value just below the onset of squares, no oscillons would appear, but an oscillon can be formed by a finite amplitude perturbation (a puff of air or a poke with a rod). When oscillons are obtained by decreasing Γ from the regime with square patterns, the number of oscillons that form is not fixed; as many as fifty oscillons were observed in the experiment in fig. 6, but no oscillons occurred if Γ was quasi-statically decreased [41].

Oscillons of like phase show a repulsive interaction that has a range not much larger than the diameter of an oscillon, while oscillons of opposite phase that are closer than about 1.4 oscillon diameters attract and form a stable dipole structure, as shown in fig. 7(a) [28,40], and more complex structures like the tetramer pictured in fig. 7(b) and the polymer chain in pictured in fig. 7(c).

Can oscillons be considered as building blocks (“atoms”) of the square lattice that forms with an increase in Γ ? This view is suggested by the observation of the formation of a square lattice as Γ is slowly increased (see fig. 7(d)): an oscillon seeds a square lattice by spawning oscillons, which adjust to form a square array. This observation suggests that the granular lattice could be modeled as a system of coupled oscillon atoms, each of which is comprised of hundreds of particles that are colliding hundreds of times during each oscillation cycle. Thus the lattice approach is much simpler than the full description

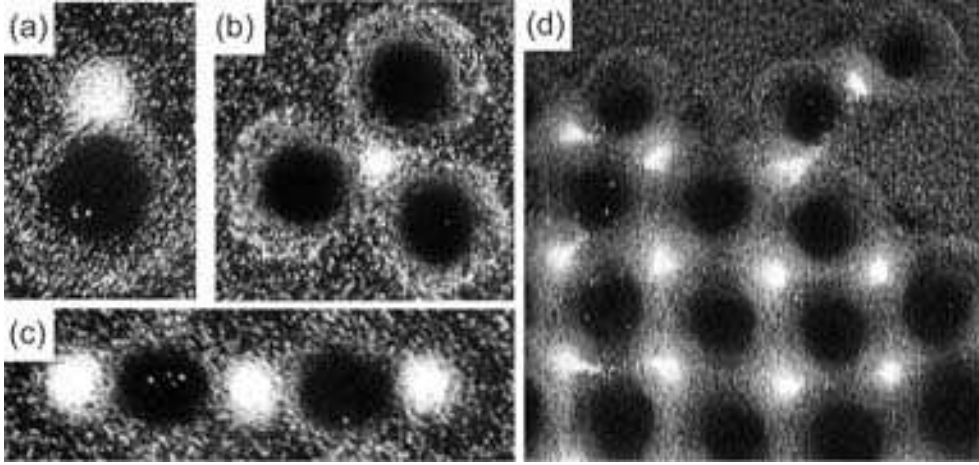


Fig. 7. – (a) Dimer formed by two bound oscillons of opposite phase; one period of oscillation of the container later the white peak will have become a crater and the black will have become a peak. (b) Tetramer formed of four oscillons. (c) Polymer chain of five oscillons. (d) A square lattice grows by nucleating oscillons. Individual bronze spheres ($\sigma = 0.165$ mm) are discernible in (a)-(c). From [28]

of all the particle motions and simpler than a continuum fluid description of the granular medium. As we will now describe, the lattice picture is supported by an analysis of the dynamics of the lattice.

Close examination of the center of mass of a peak in a square lattice reveals harmonic motion about the equilibrium position of the peak for a wide range of Γ and f [27]; such a lattice oscillation is illustrated in fig. 8. One test of the conjecture that the lattice of peaks can be modeled by a lattice of balls connected with springs is to compare the dispersion relation for the two lattices. A time sequence of images of the granular pattern was Fourier-transformed in space and then in time to obtain the frequencies of oscillations of lattice modes with different wave vectors. The frequency f_L of the lattice modes as a function of k (the magnitude of the wave vector) was found to be well described by the dispersion relation for balls connected by springs, $f_L = f_{BZ} |\sin(ka/(2\sqrt{2}))|$, where f_{BZ} is the frequency at the edge of the Brillouin zone and a the lattice spacing [27]. The lattice oscillation frequency f_L is typically an order of magnitude smaller than f but depends on the plate acceleration Γ and frequency f .

In a crystalline solid, defects form when the amplitude of oscillation of atoms about their equilibrium position in the lattice becomes large. To investigate the possible formation of defects in a granular lattice, the plate frequency f was modulated at the lattice frequency f_L . For sufficiently large modulation amplitude, defects formed, breaking the long range order of the square lattice. It was found that the amplitude of the lattice oscillations could be increased further by adding a lubricant (graphite powder) to reduce the friction between particles. The result was that the granular lattice melted [27]: the

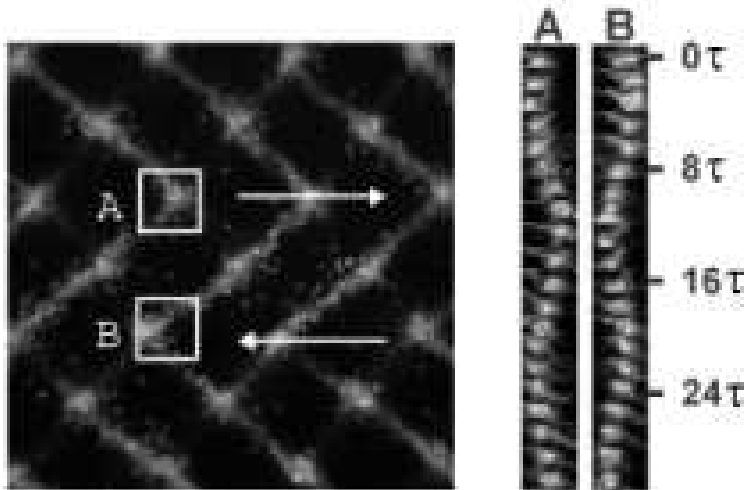


Fig. 8. – Left: close up snapshot of a granular lattice ($\Gamma = 2.9$, $f = 25$ Hz, $h = 4\sigma$). Right: time evolution of the peaks in the boxes A and B in the left-hand image. The peaks oscillate out of phase with a frequency about twenty times smaller than $f = 1/\tau$. (from [27]).

spatial Fourier transform became a circular ring (about $k = 0$) rather than sharp peaks, as fig. 9 illustrates.

Lattice oscillations and defect formation have also been studied in MD simulations, where friction can be easily varied or set to zero. First a square lattice was simulated with $\mu = 0.5$, as described previously and illustrated in the first panel of fig. 9(b). Then μ was set to zero, and defects were observed to form quickly as the lattice oscillation amplitude increased. Finally the lattice melted, as illustrated by the last panel of fig. 9(b).

Studies of melting in two-dimensional solids have shown that melting occurs when the Lindemann ratio, $\gamma = \langle |u_m - u_n|^2 \rangle / a^2$, exceeds 0.1 [42, 43]. Here u corresponds to the displacements of atoms from equilibrium lattice sites, a is the lattice constant, and the average is taken over all nearest neighbors m and n . The Lindemann ratio was computed for the granular lattice in the MD simulation, and it was found that when the friction coefficient μ was decreased, γ increased. Further, when γ reached the value 0.1 (which happened for $\mu = 0.1$ for the conditions of the simulation), the granular lattice melted, in accord with the result for crystalline solids [27].

5. – Continuum Description

Section 3 introduced Molecular Dynamics simulations as a useful tool in describing granular flows. This technique models the system on a microscopic level, evolving individual particle trajectories using Newton's laws and computing the effects of each collision. Averaging over many collisions and particle trajectories gives the macroscopic

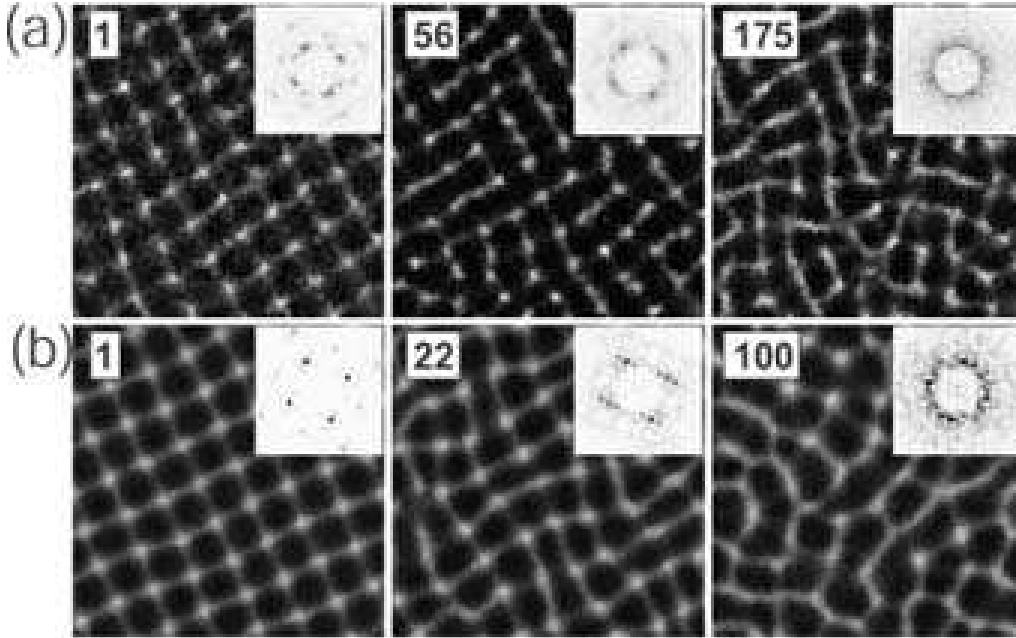


Fig. 9. – Defect creation and melting of a square granular pattern in a vertically oscillating granular layer: (a) experiment and (b) molecular dynamics simulation. The insets show Fourier transforms of the spatial patterns. In the experiment the plate oscillation frequency ($f = 32$ Hz) was modulated at the natural oscillation frequency of the lattice (2 Hz), and at $t = \tau$ graphite powder was added to the layer of bronze spheres. By $t = 56\tau$ defects had formed, and by $t = 175\tau$ the lattice had melted. In the MD simulation the friction coefficient was reduced from $\mu = 0.5$ to zero at $t = \tau$; by $t = 22\tau$ defects had formed, and by $t = 100\tau$ the lattice had melted. ($\Gamma = 2.9$.) From [27].

behavior of the flow. A complementary method for understanding granular flows is to model the macroscopic motion directly by a continuum field theory that describes the bulk motion of the flow in terms of the density, velocity and temperature fields. Unlike MD simulations, the continuum approach is not limited by particle number. A personal computer currently contains enough memory for useful MD simulations of laboratory experiments. However, industrial processes contain billions of particles, far outside the abilities of MD simulations. Another reason that a continuum approach is attractive is that it could exploit tools such as stability analysis, amplitude equations, and perturbation theory, which have been developed through more than a century of research on the the Navier-Stokes equations and other partial differential equations.

Granular flows present many difficulties in developing a continuum theory [44, 45]. Continuum theory requires a separation of length and time scales: variations over space should be small and occur over long distances, so that the behavior of local collections of

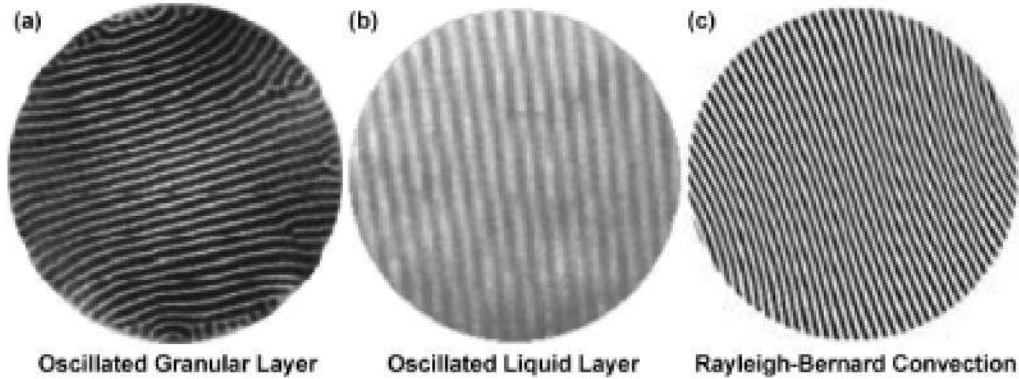


Fig. 10. – Forced granular materials produce qualitatively similar patterns as forced fluids: (a) stripe pattern formed by a vertically oscillated granular layer [26], (b) stripe pattern formed by a vertically oscillated layer of water [52], (c) stripe pattern formed in thermal convection of a fluid (CO_2) [55].

individual particles can be averaged and replaced with small fluid elements. Changes in time for the flow should occur for times long compared to the mean time between particle collision so that particles moving between fluid elements do not affect the average values in a fluid element. Unfortunately, inelastic collisions between particles create an inherent lack of scale separation [11, 45]. Sufficient separation of scales may only be present for granular flows in the specific circumstances of low density and low dissipation [11, 45, 46].

The derivation of the continuum equations from kinetic theory makes assumptions about the underlying statistics of granular flows, assumptions which have not been verified by MD simulations. For instance, the velocity distribution function is assumed to have a steady state functional form that is nearly Gaussian. Since granular flows are dissipative, a steady state distribution function can only be achieved in the presence of forcing. Granular experiments have yielded velocity distributions that depend on the forcing characteristics and experimental geometry [47-50]. Also, most derivations of continuum equations assume Boltzmann's molecular chaos (particle velocities before collisions are uncorrelated), but strong velocity correlations have been found in MD simulations [51].

Despite the reservations regarding a continuum approach in granular media, observations of granular media have revealed many phenomena similar to those observed in continuum systems. For example, the stripe patterns shown in fig. 10(a) look like those in vertically oscillated liquid layers [52] (fig. 10(b)), chemical reaction-diffusion systems [53], Rayleigh-Bénard convection in fluids [54](fig. 10(c), and liquid crystals [56].

Not only are the patterns similar for granular and continuum systems, but also some the same pattern instabilities have been observed. For example, when the wavenumber of parallel convection rolls (stripes) in a Rayleigh-Bénard convection becomes small,

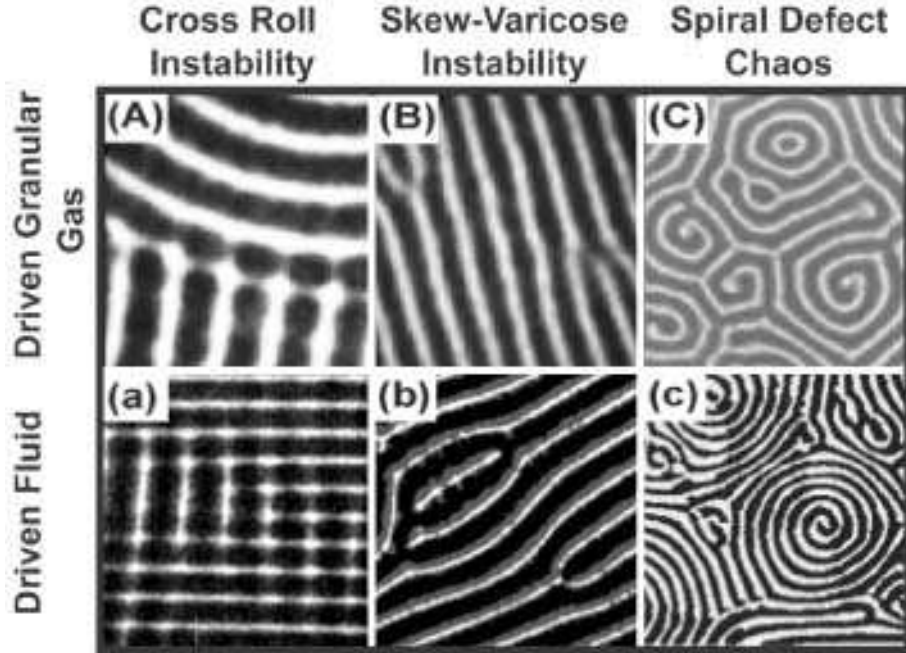


Fig. 11. – Instabilities of patterns found in oscillating granular layers and Rayleigh-Bénard convection in a fluid. Cross roll instability in stripes: (A) Vibrated granular layer [57] and (a) Rayleigh-Bénard convection [59]. Skew varicose instability in stripes: (B) Granular layer [57] and (b) Rayleigh-Bénard convection [60]. Spiral defect chaos in: (C) vibrated granular layer [61] and (c) Rayleigh-Bénard convection [60].

an instability leads to the formation of cross rolls with a larger wavenumber that are perpendicular to the original rolls [57, 58]; the same instability has been observed for stripes in oscillated granular layers, as fig. 11 illustrates. The cross rolls invade the region of small wavenumber stripes such that, after sufficient time, the region contains a pattern of straight stripes perpendicular to the original pattern and with a larger wave number.

Granular stripe patterns also exhibit a skew varicose instability like that in convection roll patterns (fig. 11). When the local wavenumber becomes too large, an initially straight pattern of stripes will develop a distortion which evolves into a dislocation defect. The defect propagates away; destroying one of the stripes and decreasing the local wave number of the pattern. The stability of the stripe pattern in fluid convection is well described by amplitude equations derived from the Navier-Stokes equations for fluids [58]. That the granular pattern shows the same behavior strongly suggests a continuum description for the vibrated system is applicable.

Aspects of the phase diagram for granular patterns (fig. 3) have been reproduced by amplitude equation models. For example, a phenomenological continuum model requiring

that the mass of the layer is conserved locally, produces stripe, square, and oscillon-like patterns similar to those found in experiment [62, 63]. A continuum, shallow water like model of the granular layer captures the patterns and yields a dispersion relation which agrees with experiment [64]. The success of these and other models [65-68] provides further motivation for considering continuum equations derived for a granular gas.

Additional evidence for the applicability of continuum theory to granular media is provided by a recent study of noise in vertically oscillating granular layers. In the Rayleigh-Bénard system below the onset of convection, thermal noise has been found to drive noisy transient disordered waves with a characteristic length scale. The intensity and coherence of these modes increases as the transition from conduction to convection is approached [69]. This behavior is well-described by the fluctuating hydrodynamic theory of Swift and Hohenberg [70]. Remarkably, the same noisy incoherent modes are observed just below the transition from a flat vertically oscillating granular layer to a square pattern [71]. The Swift-Hohenberg continuum theory describes the observations for the granular system very well, even though the noise is not thermal noise, which is many orders of magnitude too small; apparently the noise arises from the fluctuations due to the small number of particles [71].

Fired by the promise of quantitative predictive power and encouraged by the qualitative similarity of granular flows to fluid flows, researchers have proposed various continuum descriptions for rapid granular flows [72-78]. This section focuses on one such description [75] and compares results from it to MD simulations and a granular flow experiment.

Jenkins and Richmann derived a set of inelastic continuum equations in a manner similar to the derivation of the Navier-Stokes equations [75]. This approach begins with the single particle distribution function $f^{(1)}(\mathbf{r}, t)$, which gives the probability of finding a particle at a position \mathbf{r} with a velocity \mathbf{v} at a given time t . Integrating $f^{(1)}$ over all possible velocities gives the local number density, $n(\mathbf{r}, t)$. The ensemble averaged value of any particle property ψ is determined by

$$(5.1) \quad \langle \psi \rangle = \frac{1}{n} \int \psi(\mathbf{v}) f^{(1)}(\mathbf{v}, \mathbf{r}, t) d\mathbf{v}.$$

The Boltzmann equation describes how $f^{(1)}$ changes in time. Particles can move in and out of volume elements due to streaming motion; particle velocities can change in response to external forces \mathbf{F} ; or particles can be scattered out of elements by collisions. The time rate of change for $f^{(1)}$ is given by

$$(5.2) \quad \frac{\partial f^{(1)}}{\partial t} + \mathbf{v} \cdot \nabla_{\mathbf{r}} f^{(1)} + \mathbf{F} \cdot \nabla_{\mathbf{v}} f^{(1)} = \Theta(f^{(1)}),$$

where $\Theta(f^{(1)})$ is the collision operator. Collisions are considered to be binary, frictionless, and inelastic with a constant coefficient of restitution e_0 [75]. Integrating eq. (5.2) yields

the balance law for the number density,

$$(5.3) \quad \frac{\partial n}{\partial t} + \nabla \cdot (n\mathbf{u}) = 0,$$

where $\mathbf{u}(\mathbf{r}, t) = (1/n) \int \mathbf{v} f^{(1)}(\mathbf{r}, \mathbf{v}, t) d\mathbf{v}$ is the local average velocity. Multiplying by the velocity and then integrating gives the balance law for momentum,

$$(5.4) \quad n \left(\frac{\partial \mathbf{u}}{\partial t} + \mathbf{u} \cdot \nabla \mathbf{u} \right) = \nabla \cdot \mathbf{P} - ng\hat{\mathbf{z}},$$

Finally, multiplying by \mathbf{v}^2 and integrating gives the balance law for the energy, where the *granular temperature* T is proportional to the average kinetic energy of the random motion of particles,

$$(5.5) \quad T = 1/3 (\langle \mathbf{v}^2 \rangle - \langle \mathbf{v} \rangle^2),$$

$$(5.6) \quad \frac{3}{2}n \left(\frac{\partial T}{\partial t} + \mathbf{u} \cdot \nabla T \right) = -\nabla \cdot \mathbf{q} + \mathbf{P} : \mathbf{E} - \gamma.$$

The granular temperature T is many orders of magnitude greater than the Boltzmann temperature: thermal fluctuations are negligible ($mg\sigma \gg k_B T_B$).

A series of approximations is required in order to derive the form of the pressure tensor \mathbf{P} , the velocity gradient tensor \mathbf{E} , and the heat flux \mathbf{q} . One assumes that $f^{(1)}$ is nearly Gaussian, that spatial derivatives of n , \mathbf{u} , and T are small, and that $(1 - e_0)$ is small. With these assumptions, the components of the velocity gradient tensor \mathbf{E} are given by: $E_{ij} = \frac{1}{2} (\partial_j u_i + \partial_i u_j)$. The components of the stress tensor \mathbf{P} are given by the constitutive relation:

$$(5.7) \quad P_{ij} = \left[-p + \left(\lambda - \frac{2}{3}\mu \right) E_{kk} \right] \delta_{ij} + 2\mu E_{ij},$$

and the heat flux is given by Fourier's law:

$$(5.8) \quad \mathbf{q} = -\kappa \nabla T.$$

The transport coefficients are fully determined and are the same as for a dense gas of hard spheres. The bulk viscosity is given by

$$(5.9) \quad \lambda = \frac{8}{3\sqrt{\pi}} n\sigma T^{1/2} G(\nu),$$

the shear viscosity by

$$(5.10) \quad \mu = \frac{\sqrt{\pi}}{6} n \sigma T^{1/2} \left[\frac{5}{16} \frac{1}{G(\nu)} + 1 + \frac{4}{5} \left(1 + \frac{12}{\pi} \right) G(\nu) \right],$$

and the thermal conductivity by

$$(5.11) \quad \kappa = \frac{15\sqrt{\pi}}{16} n \sigma T^{1/2} \left[\frac{5}{24} \frac{1}{G(\nu)} + 1 + \frac{6}{5} \left(1 + \frac{32}{9\pi} \right) G(\nu) \right],$$

where

$$(5.12) \quad G(\nu) = \nu g_0(\nu),$$

and the radial distribution function at contact, g_0 , is [79]:

$$(5.13) \quad g_0(\nu) = \left[1 - \left(\frac{\nu}{\nu_{max}} \right)^{\frac{4}{3}\nu_{max}} \right]^{-1},$$

where ν is the volume fraction of the flow and $\nu_{max} = 0.65$ is the 3-dimensional random close-packed volume fraction.

The only difference between these equations and those for an elastic gas is γ in eq. (5.6), which accounts for the temperature loss due to inelastic collisions:

$$(5.14) \quad \gamma = \frac{12}{\sqrt{\pi}} (1 - e_0^2) \frac{n T^{3/2}}{\sigma} G(\nu).$$

The system is closed by an equation of state, proposed by Goldshtein *et al.* in [79],

$$(5.15) \quad p = nT [1 + 2(1 + e_0)G(\nu)].$$

Direct experimental verification of the inelastic continuum equations has been slow in coming due to the complexity of solving the equations and also due to difficulties in finding an appropriate experimental system [7]. The presence of strong gradients in granular materials [11, 45] adds additional difficulty to solving continuum equations. For instance, simulations of the vertically vibrated layer find that the temperature varies by three orders of magnitude throughout the cycle [80]. Thus, unlike most Navier-Stokes simulations, the transport coefficients (λ , μ and κ) cannot be treated as constants, but must be recomputed at each grid point at every time step. Additionally, a complete set of boundary conditions for granular flows is still not established and this remains an active area of research [81-86]. Without the correct boundary conditions, numerical solutions

can be unstable and are not guaranteed to converge to a correct solution in the bulk. For a good discussion on the difficulties in determining the correct boundary conditions, see Goldhirsch's review paper [11].

In a 1990 review paper [7], Campbell made a resounding call for granular flow experiments to make quantitative tests of the inelastic continuum approach. The application of new technologies such as particle tracking in two and three dimensions is now making these measurements feasible, but granular flow experiments still present technical challenges. Plugs develop in pipe flow [87,88], wall effects dominate in quasi-two-dimensional experiments [89], and detailed bulk flow measurements are difficult to make in fully three dimensional experiments [90].

The distinguishing feature of granular flows is that inelastic collisions dissipate energy. Without an external source of energy, the granular temperature decays to zero with all particles coming to rest. Experimentally, energy can only be put into the flow through the boundaries. Shock waves serve as a mechanism to deliver energy from the boundary to the bulk of the flow. Studying the balance between the transfer of energy by shock waves and the energy dissipation through inelastic collisions is important in understanding granular flows [12]. In the next section we present two studies of shock waves as a test for the inelastic continuum equations.

6. – Shock Waves in Granular Materials

The sound speed (the speed a pressure wave travels) in a granular medium is typically much smaller than the streaming velocity. Hence shocks are common in granular media. For example, imagine pouring sand out of a bucket. Gravity accelerates the flow downward, creating an average velocity U that reaches 100 cm/s after the sand has fallen by only 5 cm. In contrast, the sound speed c in the granular gas becomes small, typically 10 cm/s, as multiple particle collisions cool the gas, reducing the random velocities of the particles. The simple act of turning over a bucket full of sand can easily generate a supersonic flow with Mach number $= \frac{U}{c} = 10$. (A flow with Mach number greater than unity is supersonic.)

The sound speed in a granular gas can be determined from thermodynamic relations,

$$(6.1) \quad c = \sqrt{\left(\frac{\partial P}{\partial \rho}\right)_S} = \sqrt{\frac{c_p}{c_v} \left(\frac{\partial P}{\partial \rho}\right)_T},$$

where c is the speed of a sound, ρ is the local density, S is the entropy, c_p is the specific heat at constant pressure, and c_v is the specific heat at constant volume. For a dense inelastic gas, c is given by [91]:

$$(6.2) \quad c = \sqrt{T\chi \left(1 + \frac{2}{3}\chi + \frac{\nu}{\chi} \frac{\partial \chi}{\partial \nu}\right)},$$

where $\chi = 1 + 2(1 + e)G(\nu)$.

A shock forms when a supersonic flow encounters an obstacle. The shock separates two regions of the flow, an undisturbed region that is unaware of the obstacle, and a compressed region which has adjusted to fit the boundary conditions at the obstacle. The compressed region has a higher temperature and smaller velocity than the undisturbed region. In an ideal fluid with no viscosity, heat conduction, or dissipation, a shock is a zero-width surface of discontinuity. In a non-ideal fluid the shock has a finite width on the order of a particle's mean free path in the fluid [92].

When a fluid with velocity $U > c$ impinges perpendicularly onto an obstacle, a *normal* shock forms and propagates in the $-U$ direction. Section 6.2 will discuss the formation and propagation of normal shocks in a vertically vibrated granular layer where the flow fields and thus the shocks are highly time dependent [80]. If, instead, the fluid velocity and the obstacle are not perpendicular, an *oblique* shock forms and propagates into the flow at an angle and with a speed determined by the local flow values. Section 6.1 describes an oblique shock formed in a steady state laboratory flow past a wedge [89].

6.1. Steady state flow past an obstacle. – We now describe an experimental study of shocks in a time-independent flow, and then the experimental results will be compared to two simulations: an event-driven molecular dynamics simulation, similar to those discussed in Section 3, and a two-dimensional, finite-element solution of the inelastic continuum equations presented in Section 5.

In the experiment, stainless steel spheres (particle diameter $\sigma = 1.2$ mm) fell under gravity past a wedge sandwiched between two glass plates separated by 1.6σ . The particles were initially distributed uniformly on a conveyor belt. As the conveyor turned, particles fell off into a hopper that guided the particles into the cell formed of the closely spaced plates; the wedge was located a distance of 42σ below the top of the cell. The positions and velocities of the particles were determined from high speed images of the falling particles, and data from many thousands of particles were averaged to obtain the time-independent velocity, volume fraction, and temperature fields. The average free stream speed of sound determined from the measurements for flow incident on the wedge was 0.09 m/s. The flow entered the top of the cell with a Mach number of 7 and accelerated under gravity to a Mach number of 12 at the tip of the wedge.

The horizontal velocity field measured in the experiment is shown in fig. 12(a). A shock separates the undisturbed region, where the horizontal velocity is nearly zero, from the compressed region, whose stream lines follow the flow around the obstacle. Because of gravity and inelasticity, the shock does not extend out at a constant angle but curves towards the wedge.

At the bottom of the wedge the compressed gas expands in a fan-like structure as the volume available to the flow increases (fig. 13). In an expansion fan the density and temperature decrease and the Mach number increases. The expansion fan is a smooth transition radiating from the bottom corner of the wedge.

The flow was computed numerically in a three-dimensional MD simulation (fig. 12(b)) and in a two-dimensional finite difference simulation of the inelastic continuum equations

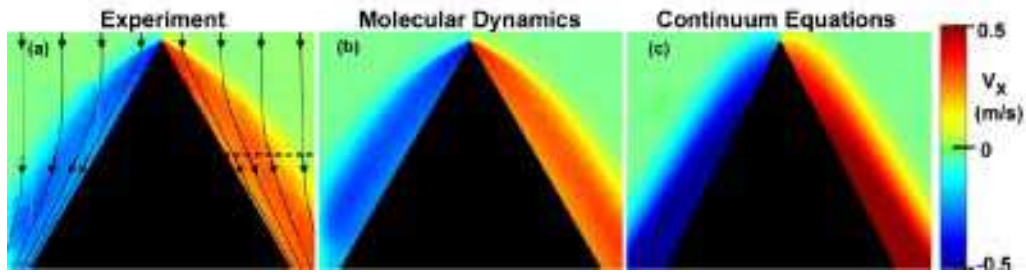


Fig. 12. – Horizontal component of the velocity field of a granular flow incident downward on a wedge, determined by three methods: (a) experiment, (b) MD simulations, and (c) integration of inelastic continuum equations. Each picture shows a region 130σ by 104σ . The solid lines with arrows denote streamlines. Quantitative comparisons along the dashed line in (a) are shown in figs. 14 and 15. (From [89]).

(fig. 12(c)). The two simulations yield results for the horizontal component of velocity in qualitative accord with experiment: a shock forms at the tip of the obstacle, and behind the shock the flow is compressed, has a higher temperature, and lower mean velocity. Quantitative comparisons among the methods are plotted for values of the fields along the dashed line shown in fig. 12(a).

Three parameters were adjusted in the MD simulation to achieve the agreement with the experiment shown in figs. 14. The same coefficient of restitution $e_0 = 0.97$ and friction coefficient $\mu = 0.15$ were used to model interparticle and particle-wall collisions.

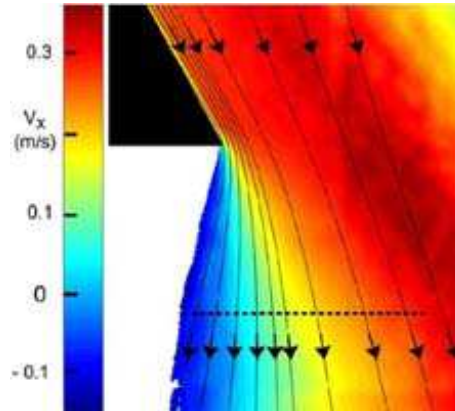


Fig. 13. – The horizontal velocity field measured for the expansion fan that formed when the supersonic granular flow reached the bottom of the wedge. The solid lines indicate selected streamlines. The total height of the region shown is 55σ . The white region below the wedge had too few particles for the velocity to be determined. (From [89])

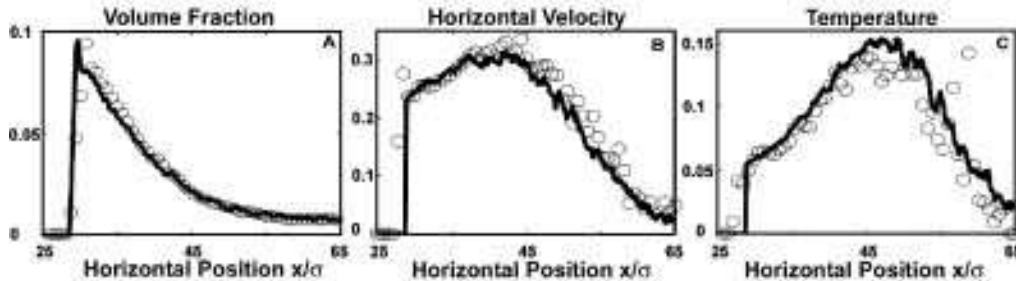


Fig. 14. – Shock profiles for granular flow past a wedge measured in an experiment (circles) are compared with results from molecular dynamics (solid lines): (a) volume fraction, (b) horizontal component of the velocity, and (c) temperature. The profiles are taken along the dashed line in fig. 12. (From [89])

The initial conditions of the experiment were modeled by placing particles into the top of the cell at a constant rate. Incoming particles were placed randomly at the top of the cell with a mean downward velocity measured from the experiment, and fluctuations were chosen from a Gaussian distribution determined by the measured temperature. An additional parameter α , defined as the ratio of temperature perpendicular to the wall to that parallel to the wall, was set to 0.8. These parameters, which were not measured in the experiment, were adjusted to provide agreement in the full flow fields, including the free-stream velocity.

Results from the MD simulation are compared with experiment in fig. 14 for the volume fraction, horizontal velocity component, and temperature. The agreement is quite good with a root mean square difference between experiment and simulation of less than 2% for the volume fraction and velocity fields and 10% for the temperature field.

The simple geometry and steady state behavior of the experiment provided a good system for testing the inelastic continuum equations. However, a full three-dimensional simulation of the experiment was found to be time prohibitive. Instead, the equations were solved on a two-dimensional grid; consequently the simulation could not capture the interaction of particles with the confining glass side walls. Frictional collisions with the side walls strongly affected the flow in the experiment and in the fully three-dimensional MD simulations. The average downward acceleration of a single particle falling between the two glass plates in the experiment was 8.9 m/s^2 , while the same particle falling outside the cell accelerated with the expected 9.8 m/s^2 .

The continuum equations were numerically solved by a second-order accurate, finite difference method. The only fit parameter in the equations was the coefficient of restitution, which was set to the same value of $e_0(0.97)$ used in the MD simulation. Boundary conditions at the inlet were determined by the experiment and at the outlet were free. Slip velocity boundary conditions were used along the wedge boundary. The heat flux at the wedge was taken to be proportional to the local ν and $T^{3/2}$ [85]. Euler time stepping

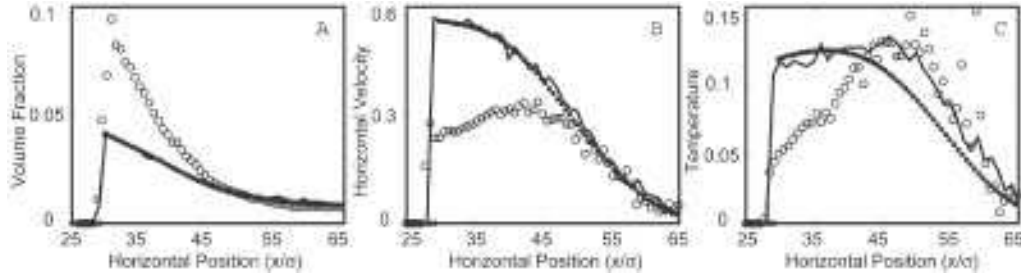


Fig. 15. – Comparison of shock profiles for granular flow past a wedge obtained from molecular dynamics (solid lines) and inelastic continuum equations (dotted line), assuming no friction. (a) Volume fraction, (b) horizontal velocity profile, and (c) temperature along the dashed line in fig. 12(a). Experimental measurements (open circles) show similar qualitative behavior but disagree quantitatively. The difference between the simulations and the experiment is due to wall friction. (From [89])

was used to increment the simulation until the flow reached a steady state where the horizontally averaged mass flux was constant to 0.01

Experiment and continuum simulation showed similar behavior, but the shape of the curves differed and the magnitudes of the fields disagreed by as much as a factor of two (fig. 15). This disagreement was attributed to the frictional drag of the confining side walls in the experiment. A three-dimensional simulation of the inelastic continuum equations with viscous boundary conditions along the side walls should agree better with the experiment [12].

Molecular dynamics simulations were done with wall drag neglected for comparison with the two-dimensional simulation of the continuum equations. The two simulations agreed remarkably well in all regions of the flow except within 5σ of the wedge tip. Near the tip of the wedge, the two simulations disagreed due to different boundary conditions. The agreement between the two simulations in the bulk of the flow confirms the applicability of the continuum description for granular flows. The disagreement with the experiment emphasizes once again the importance of including friction in a continuum description, both in the equations and in the boundary conditions.

6.2. Shock waves in a vertically oscillating layer. – Section 2 described the patterns that form when a layer of granular materials is vertically oscillated. Shocks play an important role in this system [80]. Each time the layer collides with the plate a shock forms and propagates through the layer, transmitting energy upward through the layer to the surface. The striking similarity of the granular patterns to their counterparts in continuum systems strongly suggests that a continuum description of granular flows could prove useful. If this is true, the continuum description must also capture the shock dynamics in the bulk of the layer.

Here we compare inelastic, frictionless, fully three-dimensional MD and continuum

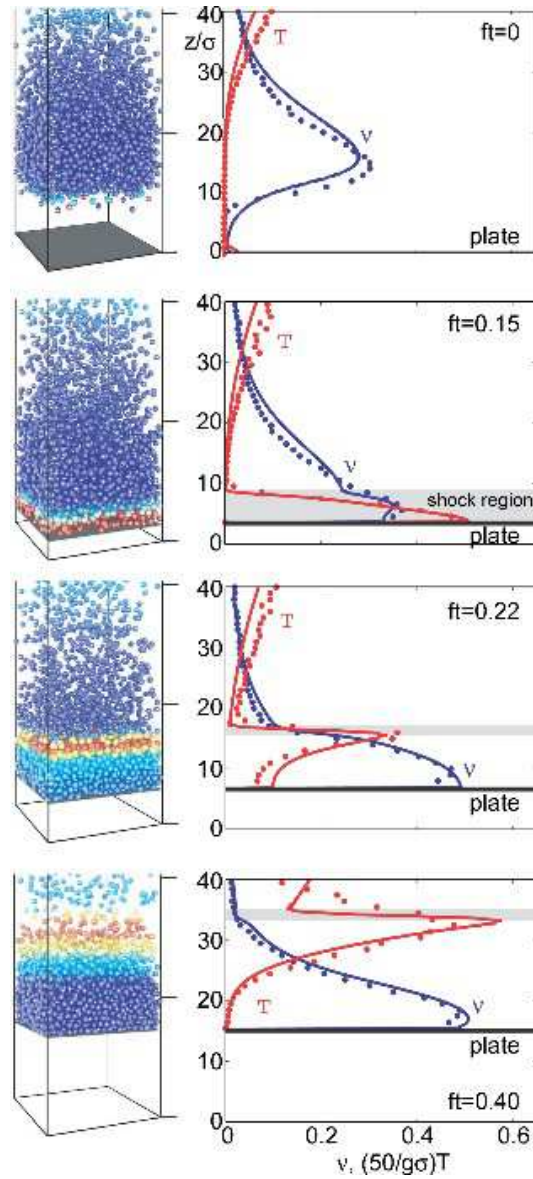


Fig. 16. – Dimensionless temperature $T/g\sigma$ and volume fraction ν as functions of the dimensionless height z/σ at four times ft in the oscillation cycle. For each time, a snap shot from the MD simulation is shown in the left column, with individual particles color coded according to temperature: high T in red, low T in blue, and the bottom plate of the container shaded solid gray. The right column shows horizontally averaged ν (blue) and $T/g\sigma$ (red) for the same four times. The plate is shown as a horizontal black solid line, results from MD simulation are shown as dots, and continuum results are solid lines (From [80]).

simulations. In order to focus on the formation and propagation of the shock wave, pattern formation is intentionally suppressed by considering a container smaller than one wavelength of the pattern in either horizontal direction. We focus on one point in the phase space shown in fig. 3: $\Gamma = 3$ and $f^* = 0.42$ for a layer with depth $h = 9\sigma$. For this set of parameter values, a vibrated layer in a larger cell would have a $f/2$ stripe pattern.

In both simulations periodic boundary conditions were used in the two horizontal directions and impermeable boundary conditions, $u_z = 0$, were applied at the plate. The additional boundary conditions required for the continuum simulations were taken from the MD simulation. In the MD simulation, the vertical derivatives at the plate were negligible throughout most of the cycle. For simplicity, the continuum simulation assumed $\partial u_x/\partial z = 0$, $\partial u_y/\partial z = 0$, and $\partial T/\partial z = 0$ at all times in the cycle.

The evolution of the shock wave throughout a plate cycle is shown in figs. 16 and 17. The dynamics of the cycle occurs in the time interval between $ft = 0$ and one cycle later, $ft = 1$.

At $ft = 0$ the container is at its minimum height. The layer, having been thrown off the plate in the previous cycle, now falls towards the plate. Inelasticity has dissipated most of the energy so that the layer's temperature is nearly zero. The Mach number of the layer with respect to the plate is much greater than one. The MD and continuum simulation show similar behavior in the v and T fields.

At $ft = 15$ the layer begins to collide with the plate. A shock wave forms, separating the region near the plate where ν and T increases from the undisturbed region still falling towards the plate.

At $ft = 0.22$ the shock wave is moving through the layer. The compressed region continues to grow. Collisions between particles in this high density region cause the layer to cool behind the shock, creating a lower temperature near the plate.

At $ft = 0.40$ the shock has propagated through the layer and into the very dilute region above the layer. At this time, the plate is approaching its maximum height and the layer begins to leave the plate as the downward plate acceleration exceeds g . The layer continues to cool behind the shock, setting the stage for the next oscillation.

The MD and continuum simulations show good agreement throughout the cycle, despite the presence of large spatial gradients and a strong time dependence. In the dilute regimes above and below the layer, numerical solutions of the inelastic continuum equations are unstable unless artificial dissipation is added [80], following the example from numerical solutions of Knudsen gases. [93]. The effect of the extra dissipation is most pronounced in the falling layer and accounts for the disagreement between MD and continuum at the top of the cell.

Inelastic collisions between particles are the distinguishing characteristics of a granular gas, but few studies have examined how granular flow properties depend on the restitution coefficient. Simulations for the oscillating layer were modified to study the effect of varying e_0 on the propagation of the shock. The initial conditions for this numerical experiment were taken for a layer with $e_0 = 0.99$, using the same parameters as in the above discussion. At $ft = 0.33$, when the center of mass layer was near its maximum

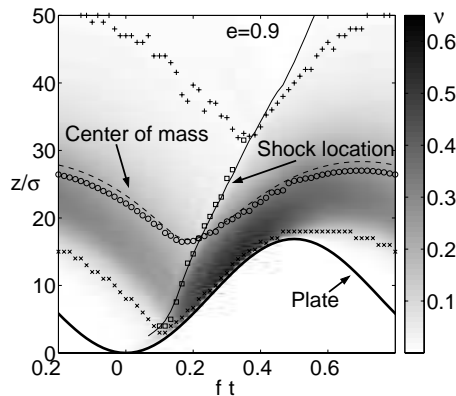


Fig. 17. – Location of the shock (solid line for continuum, squares for MD) and the center of mass of the layer (dashed line for continuum, circles for MD) as a function of time ft during one cycle of the plate (thick solid line) for particles with $e_0 = 0.90$. The plot is shaded according to the volume fraction from the continuum simulation, so that high volume fraction is dark and low volume fraction is light. The “top” and the “bottom” of the layer from MD (when the volume fraction drops to less than 4% of that for random close packed particles) are shown as +’s and X’s respectively. The material below the shock is compressed as compared to the region above the shock, as can be seen from the shading. From [80].

height above the plate, the coefficient of restitution was suddenly changed, which changed the subsequent evolution of the shock.

As before, when the layer hits the plate it compresses and forms a shock that propagates through the layer. The smaller the value of e_0 , the faster the layer cools and compacts; for small e_0 , the layer remains very compact throughout the cycle and leaves the plate almost as a solid body. For higher values of e_0 , the layer dilates quickly after each collision with the plate. The maximum height of the center of mass in a cycle increases with increasing e_0 .

The speed of the shock (eq. (6)) depends on both the temperature of the flow and on its density. Since the density and temperature of the flow change throughout the cycle, so does the shock speed as the shock propagates through the layer. The behavior of the average speed of the shock as a function of inelasticity is shown in fig. 18. For small values of e_0 the shock speed asymptotes to a fixed value of $47\sqrt{g\sigma}$. The shock speed monotonically increases with increasing e_0 . The special case of elastic particles appears to match with the limit of $e \rightarrow 1$, suggesting that there is no qualitative difference in shock propagation through elastic and inelastic gases.

For both problems we have considered – granular flow past a wedge and a vertically oscillating granular layer – numerical solutions of the inelastic continuum equations of Jenkins and Richman agree well with MD simulations for frictionless particles. The continuum equations were derived for a weakly dissipative, low density, frictionless granular

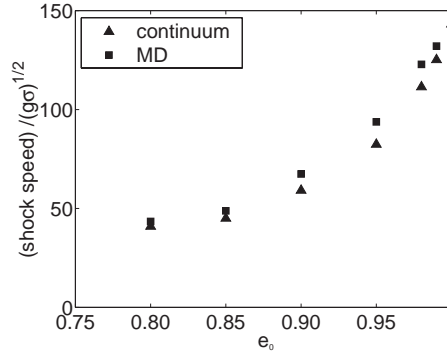


Fig. 18. – Average dimensionless shock speed, $v_{shock}/\sqrt{g\sigma}$, in the reference frame of the plate. v_{shock} is calculated as the average speed of the shock from when the shock is formed until it leaves the layer. (From [80])

gas, assuming small gradients in the flow fields in both space and time. Nevertheless, the equations capture the evolution of a shock through a dense, inelastic oscillating layer, and qualitatively capture the properties of a shock formed in flow past a wedge. With more research on boundary conditions and the incorporation of friction, these continuum equations show great promise.

7. – Discussion

More than one thousand papers have been published on granular materials since de Gennes brought the subject to the attention of physicists, and Bak’s work (1987) on self-organized criticality stimulated interest in sand piles [94]. However, much remains to be done to achieve a level of understanding of granular media comparable to that for fluids and crystalline solids. Experiments and simulations have investigated a wide range of problems including the angle of repose [95] and internal structure of sand piles [96,97], shear forces in Couette-Taylor flows [90,98], convection due to temperature gradients [99-101] and due to buoyancy [102], flows in a rotating drum [103,104], and chute flows [31, 105-107]. Much of the research has concerned granular media as a solid where particles are in continuous contact, while this chapter has concerned rapid granular flows (the “collisional regime”) where inertial effects are important and force chains do not play a major role. We have further limited the considerations to particles that interact only on contact.

Understanding flows of grains that interact only on contact would seem at first to involve a straightforward application of Newton’s laws. However, the energy loss in collisions complicates the application of standard statistical methods. We have focused on two systems that hint at the rich variety of phenomena exhibited by granular media in the collisional regime: a vertically vibrated granular layer and supersonic granular flow

past an obstacle. These two problems were chosen because they are amenable to direct comparison of experiment, molecular dynamics simulations, and continuum theory.

A vertically vibrated granular layer spontaneously forms spatially extended patterns. Experiments and MD simulations reveal that the collective motion of grains arises due to dissipative collisions between particles, and does not require mediation by an interstitial gas or side walls. For square granular patterns, an approach intermediate between molecular dynamics and continuum models has been found to describe the dynamics of the lattice pattern: a collection of particles that form a peak (an oscillon) is like an atom in a crystalline lattice. The modes of the granular lattice obey the dispersion relation for a two-dimensional lattice, and the granular lattice even forms defects and melts in the same way as a two-dimensional crystal of atoms (Section 2).

The spatial patterns formed by oscillating granular layers exhibit marked similarities to those observed in continuum nonequilibrium systems such as convecting fluids and oscillating liquids (Section 5). Further, the cross-roll and skew-varicose instabilities observed in thermal convection in a fluid and interpreted in terms of the hydrodynamic equations (more specifically, the Boussinesq equations) have also been observed in oscillated granular layers. Various amplitude equation models have been found to describe granular patterns and their instabilities. Even the subtle effects of noise on the transition from conduction to convection in fluids have been found also in oscillating granular layers near the onset of the transition from a flat layer to a square pattern.

The striking similarities of granular patterns to those found in nonequilibrium continuum systems and in experiments on granular flows under shear and in rotating drums suggest that granular gases may be describable by continuum theory. Inspired by these observations, researchers have proposed many continuum descriptions. The descriptions differ in the particle properties included in the collision model; for instance, collision models can be frictionless [75,108] or can account for friction between particles [109,110]. Equations of motion obtained by Goldshtein and Shapiro include, in addition to the terms in the Navier-Stokes equation, a term accounting for heat transport by density gradients [76]. A Model presented by Bocquet *et al.* [90] includes corrections to the viscosity due to velocity correlations. None of these models has been definitively established.

We have compared predictions of continuum equations derived by Jenkins and Richman with experiments on shocks in vibrating layers and flow past an obstacle. For both geometries, numerical solutions of the inelastic continuum equations agree well with results from MD simulations of smooth (frictionless) inelastic spheres. However, comparisons of the continuum equations with experiment and with MD simulations for particles with friction have demonstrated the crucial role of friction in granular flows. For continuum equations to achieve quantitative predictive power, the effects of friction between particles and between particles and boundaries must be included.

Derivations of granular hydrodynamic equations have thus far assumed weak dissipation and small particle volume fractions. Future work should extend theory to higher densities and larger dissipation. Because inelastic collisions dissipate temperature, granular flows frequently coexist with solid-like sand piles. A major challenge is the development of theory that bridges the gap from the collisional regime to the quasi-static regime

where particles are always in contact.

As continuum equations of motion become better established, it will become possible to exploit the power of the continuum description. Continuum models for larger and denser systems may reveal new phenomena. Continuum simulations are better suited to time-dependent flows than MD simulations. Linear and nonlinear stability analyses could provide insight into bifurcations, just as a century of stability analyses of the Navier-Stokes equations has given insights into diverse fluid flow phenomena. Stability analyses have been conducted for simplified continuum models (see, e.g., [111]), but thus far no stability analysis has been conducted for a realistic set of granular hydrodynamic equations. Further, given a set of granular equations like the Navier-Stokes equations, it should be possible to derive amplitude equations, which can yield a better understanding of instabilities in granular flows.

The experiments and theory presented in this chapter involve spheres of uniform size, while industrial applications usually involve a wide range of particle sizes and shapes. Experiments and simulations on flows with two particle sizes show an additional richness to granular flow phenomena such as size segregation [23, 112-115], nonequipartition of energy [116, 117], and increased normal stress [117]. Much theoretical and experimental work is needed on systems of particles with a range of sizes and shapes.

Air friction is usually neglected in simulations and in the interpretation of experiments, whether or not the experiments are conducted in vacuum. In contrast, in granular systems in industry, air friction and buoyancy are often important, although the air effects can be negligible for large particles (say greater than 1 mm). The interaction of the interstitial fluid and sand leads to the development of sand dunes [118] and sand ripples [119, 120] and the formation of heaps in vibrated layers [121]. The inclusion of interstitial flow in continuum theories for granular materials is another challenge for future research on granular materials.

In conclusion, much remains to be done to establish a fundamental understanding granular flows. Future studies should seek more examples of granular flows amenable to experiment, molecular dynamics simulations, and continuum theory. A concerted attack from three approaches should lead to a better understanding of outstanding issues concerning boundary conditions, the incorporation of particle friction and velocity correlations into theory, and the extension of theory to higher particle volume fractions and higher dissipation.

8. – Acknowledgments

In the past two decades granular media have been studied by many scientists. For convenience, our examples have been taken largely from research in the Center for Non-linear Dynamics at The University of Texas at Austin (see <http://chaos.utexas.edu>). We thank particularly Chris Bizon, Jonathan Bougie, Francisco Melo, Daniel Goldman, W. D. McCormick, Sung Joon Moon, Mark Shattuck, Jack Swift, and Paul Umbanhowar. This research was supported by the Engineering Research Program of the Office of Basic Energy Sciences of the U.S. Department of Energy and the Texas Advanced Research

Program.

REFERENCES

- [1] ENNIS B.J., GREEN J. and DAVIES R., *Chemical Engineering Progress*, **90**, (1994) 32.
- [2] FARADAY M., *Philos. Trans. R. Soc. London*, **121**, (1831) 299.
- [3] EVESQUE P. and RAJCHENBACH J., *Phys. Rev. Lett.*, **62**, (1989) 44.
- [4] FAUVE S., DOUADY S. and LAROCHE C., *Physica Scripta*, **T29**, (1989) 250.
- [5] DOUADY S., FAUVE S. and LAROCHE C., *Europhysics Letters*, **8**, (1989) 621.
- [6] DE GENNES P.G., *Rev. Mod. Phys.*, **71**, (1999) S374.
- [7] CAMPBELL C.S., *Annu. Rev. Fluid Mech.*, **2**, (1990) 57.
- [8] JAEGER H.M. and NAGEL S.R., *Science*, **255**, (1992) 1523.
- [9] JAEGER H.M., NAGEL S.R. and BEHRINGER R.P., *Physics Today*, **49**,no. 4 (1996) 32.
- [10] RAJCHENBACH J., *Advances in Physics*, **49**, (2000) 229.
- [11] GOLDBIRSCHE I., *Annu. Rev. Fluid Mech.*, **35**, (2003) 267.
- [12] GOLDSHTEIN A., ALEXEEV A. and SHAPIRO M., in *Granular Gas Dynamics*, edited by T. POSCHEL and N. BRILLIANTOV (Springer, Berlin) (2003), pp. 188–225.
- [13] XU H., LOUGE M. and REEVES A., *Continuum Mech. Thermodyn.*, **15**, (2003) 321.
- [14] BAGNOLD R.A., *Proc. Royal Soc. London*, **49**, (1954) 225.
- [15] BIDEAU D. and HANSEN A. (Editors), *Disorder and Granular Media* (Elsevier, Amsterdam) (1993).
- [16] DURAN J., *Sands, Powders, and Grains: An Introduction to the Physics of Granular Materials* (Springer, Berlin) (2000).
- [17] POSCHEL T., *Granular Cases, Lecture Notes in Physics* (Cambridge University Press, Cambridge) (2003).
- [18] POSCHEL T. and BRILLIANTOV N. (Editors), *Granular Glass Dynamics* (Springer, Berlin) (2003).
- [19] GOLDSMITH W., *Impact* (Edward Arnold Ltd., London) (1960).
- [20] LORENZ A., TUOZZOLO C. and LOUGE M., *Experimental Mechanics*, **37**, (1997) 292.
- [21] PICA C., LARA A., LEE A., GOLDMAN D. and SWINNEY H., in *The Physics of Complex Systems (New Advances and Perspectives)—the International School of Physics Enrico Fermi*, edited by F. MALLAMACE and E. STANLEY (Italian Physical Society) (2004).
- [22] PICA C., LARA A., LEE A., GOLDMAN D., VISHIK I. and SWINNEY H., *Phys. Rev. Lett.*, **92** (2004) 194301.
- [23] MOON S.J., GOLDMAN D.I., SWIFT J.B. and SWINNEY H.L., *Phys. Rev. E*, **69**, (2004) 031301.
- [24] UMBANHOWAR P. and SWINNEY H.L., *Physica A*, **288**, (2000) 344.
- [25] BIZON C., SHATTUCK M.D., SWIFT J.B., MCCORMICK W.D. and SWINNEY H.L., *Phys. Rev. Lett.*, **80**, (1998) 57.
- [26] MELO F., UMBANHOWAR P.B. and SWINNEY H.L., *Phys. Rev. Lett.*, **75**, (1995) 3838.
- [27] GOLDMAN D.I., MOON S.J., SWIFT J.B. and SWINNEY H.L., *Phys. Rev. Lett.*, **90**, (2003) 104302.
- [28] UMBANHOWAR P., MELO F. and SWINNEY H.L., *Nature*, **382**, (1996) 793.
- [29] MOON S.J., SHATTUCK M.D., BIZON C., GOLDMAN D.I., SWIFT J.B. and SWINNEY H.L., *Phys. Rev. E*, **65**, (2002) 011301.

- [30] MEHTA A. and LUCK J.M., *Phys. Rev. Lett.*, **65**, (1990) 393.
- [31] CAMPBELL C.S. and BRENNEN C.E., *Trans. ASME E: J. Appl. Mech.*, **52**, (1985) 172.
- [32] RAPAPORT D., *The Art of Molecular Dynamics Simulation* (Cambridge University Press, Cambridge) (1995).
- [33] WALTON O.R., in *Particulate Two-Phase Flow*, edited by M.C. ROCO (Butterworth-Heinemann, Boston) (1993), pp. 884–911.
- [34] MCNAMARA S. and YOUNG W.R., *Phys. Fluids A*, **4**, (1992) 496.
- [35] LUDING S., CLÉMENT E., RAJCHENBACH J. and DURAN J., *Europhys. Lett.*, **36**, (1996) 247.
- [36] GOLDMAN D., SHATTUCK M.D., BIZON C., MCCORMICK W.D., SWIFT J.B. and SWINNEY H.L., *Phys. Rev. E*, **57**, (1998) 4831.
- [37] ARGENTINA M., CLERC M. and SOTO R., *Phys. Rev. Lett.*, **89**, (2002) 044301.
- [38] NIE X., BEN-NAIM E. and CHEN S., *Phys. Rev. Lett.*, **89**, (2002) 204301.
- [39] KHAIN E. and MEERSON B., *Phys. Rev. E*, **67**, (2003) 021306.
- [40] UMBANHOWAR P.B., MELO F. and SWINNEY H.L., *Physica A*, **249**, (1998) 1.
- [41] UMBANHOWAR P.B., *Wave Patterns in Vibrated Granular Layers*, Ph.D. thesis, University of Texas at Austin (1996).
- [42] BEDANOV V.M., GADIYAK G.V. and LOZOVIK Y.F., *Phys. Lett. A*, **109A**, (1985) 289.
- [43] ZHENG X.H. and EARNSHAW J.C., *Europhys. Lett.*, **41**, (1998) 635.
- [44] ZHOU T. and KADANOFF L.P., *Phys. Rev. E*, **54**, (1996) 623.
- [45] TAN M.L. and GOLDBIRSH I., *Phys. Rev. Lett.*, **81**, (1998) 3022.
- [46] KADANOFF L.P., *Rev. Mod. Phys.*, **71**, (1999) 435.
- [47] OLAFSEN J. and URBACH J.S., *Phys. Rev. E*, **60**, (1999) 4268.
- [48] KUDROLLI A. and HENRY J., *Phys. Rev. E*, **62**, (2000) 1489.
- [49] VEJE C.T., HOWELL D.W. and BEHRINGER R.P., *Phys. Rev. E*, **59**, (1999) 739.
- [50] ROUYER F. and MENON N., *Phys. Rev. Lett.*, **85**, (2000) 3676.
- [51] MOON S.J., SHATTUCK M.D. and SWIFT J.B., *Phys. Rev. E*, **64**, (2001) 31303.
- [52] KUDROLLI A. and GOLLUB J.P., *Physica D*, **97**, (1996) 133.
- [53] OUYANG Q. and SWINNEY H., *Nature*, **352**, (1991) 610.
- [54] BEHRINGER R., *Rev. Mod. Phys.*, **57**, (1985) 657.
- [55] PLAPP B., private communication.
- [56] DUBOIS-VIOLETTE E., DUNRAND G., GUYON E., MANNEVILLE P. and PIERANSKI P., in *Liquid Crystals*, edited by L. LIEBERT (Academic Press, New York) (1978), p. 147.
- [57] DE BRUYN J.R., BIZON C., SHATTUCK M.D., GOLDMAN D., SWIFT J.B. and SWINNEY H.L., *Phys. Rev. Lett.*, **81**, (1998) 1421.
- [58] CROSS M.C. and HOHENBERG P.C., *Rev. Mod. Phys.*, **65**, (1993) 851.
- [59] BUSSE F.H. and WHITEHEAD J.A., *J. Fluid Mech.*, **47**, (1971) 305.
- [60] ASSENHEIMER M. and STEINBERG V., *Phys. Rev. Lett.*, **70**, (1993) 3888.
- [61] DE BRUYN J.R., LEWIS B.C., SHATTUCK M.D., SWIFT J.B. and SWINNEY H.L., *Phys. Rev. E*, **63**, (2001) 041305.
- [62] TSIMRING L. and ARONSON I., *Phys. Rev. Lett.*, **79**, (1997) 213.
- [63] CERDA E., MELO F. and RICA S., *Phys. Rev. Lett.*, **79**, (1998) 4570.
- [64] EGGERS J. and RIECKE H., *Phys. Rev. E*, **59**, (1999) 4476.
- [65] SHINBROT T., *Nature*, **389**, (1997) 574.
- [66] SAKAGUCHI H. and BRAND H.R., *J. de Phys. II*, **7**, (1997) 1325.
- [67] ROTHMAN D.H., *Phys. Rev. E*, **57**, (1998) R1239.
- [68] VENKATARAMANI S.C. and OTT E., *Phys. Rev. Lett.*, **80**, (1998) 3498.

- [69] OH J. and ALHERS G., *Phys. Rev. Lett.*, **91**, (2003) 094501.
- [70] SWIFT J. and HOHENBERG P., *Phys. Rev. A*, **15**, (1977) 319.
- [71] GOLDMAN D.I., SWIFT J.B. and SWINNEY H.L., *Phys. Rev. Lett.*, **92**, (2004) 174302.
- [72] HAFF P.K., *J. Fluid Mech.*, **134**, (1983) 401.
- [73] AHMADI G. and SHAHINPOOR M., *Int. J. Non-linear Mechanics*, **19**, (1983) 177.
- [74] LUN C.K.K., *J. Appl. Mech.*, **54**, (1987) 47.
- [75] JENKINS J.T. and RICHMAN M.W., *Arch. Rat. Mech. Anal.*, **87**, (1985) 355.
- [76] GOLDSHTEIN A. and SHAPIRO M., *J. Fluid Mech.*, **282**, (1995) 75.
- [77] SELA N., GOLDSHIRSCH I. and NOSKOWICZ S.H., *Phys. Fluids*, **8**, (1996) 2337.
- [78] BREY J.J., DUFTY J.W. and SANTOS A., *J. Stat. Phys.*, **87**, (1997) 1051.
- [79] GOLDSHTEIN A., SHAPIRO M. and GUTFINGER C., *J. Fluid Mech.*, **327**, (1996) 117.
- [80] BOUGIE J., MOON S.J., SWIFT J.B. and SWINNEY H.L., *Phys. Rev. E*, **66**, (2002) 1.
- [81] SILBERT L., GRETT G. and PLIMPTON S., *Phys. Fluids*, **14**, (2002) 2637.
- [82] SOTO R. and MANSOUR M., *Physica A*, **327**, (2003) 88.
- [83] JENKINS J.T., *Transactions of the ASME*, **59**, (1992) 120.
- [84] JENKINS J. and ASKARI E., *Chaos*, **9**, (1999) 654.
- [85] JENKINS J.T. and LOUGE M.Y., *Phys. Fluids*, **9**, (1997) 2835.
- [86] BREY J., RUIZ-MONTERO M. and MORENO F., *Phys. Rev. E*, **62**, (2000) 5339.
- [87] AIDER J.L., SOMMIER N., RAAFAT T. and HULIN J.P., *Phys. Rev. E*, **59**, (1998) 778.
- [88] PÖSCHEL T., *J. Phys. II France*, **3**, (1993) 27.
- [89] RERICHA E.C., BIZON C., SHATTUCK M.D. and SWINNEY H.L., *Phys. Rev. Lett.*, **88**, (2002) 014302.
- [90] BOCQUET L., LOSERT W., SCHALK D., LUBENSKY T. and GOLLUB J., *Phys. Rev. E*, **65**, (2001) 011307.
- [91] SAVAGE S.B., *J. Fluid Mech.*, **194**, (1988) 457.
- [92] ANDERSON J.D., *Modern Compressible Flow with Historical Perspective* (McGraw-Hill, Boston) (1990).
- [93] ROACHE P., *Computational Fluid Dynamics* (Hermosa Publishers, Albuquerque) (1976).
- [94] BAK P., TANG C. and WIESENFELD K., *Phys. Rev. Lett.*, **59**, (1987) 381.
- [95] JAEGER H.M., LIU C. and NAGEL S.R., *Phys. Rev. Lett.*, **62**, (1989) 40.
- [96] MEHTA A. and BARKER G.C., *Rep. Prog. Phys.*, (1994) 383.
- [97] VANEL L., HOWELL D., CLARK D., BEHRINGER R. and CLEMENT E., *Phys. Rev. E*, **60**, (1999) R5040.
- [98] HOWELL D., BEHRINGER R.P. and VEJE C., *Phys. Rev. Lett.*, **82**, (1998) 5241.
- [99] HAYAKAWA H., YUE S. and HONG D.C., *Phys. Rev. Lett.*, **75**, (1995) 2328.
- [100] RAMIREZ R., RISSO D. and CORDERO P., *Phys. Rev. Lett.*, **85**, (2000) 1230.
- [101] EHRICHS E.E., JAEGER H.M., KARCZMAR G.S., KNIGHT J.B., KUPERMAN V.Y. and NAGEL S.R., *Science*, **267**, (1995) 1632.
- [102] CORDERO P., RAMIREZ R. and RISSO D., *Physica A*, **327**, (2003) 82.
- [103] SHEN A., *Physics of Fluids*, **14**, (2002) 462.
- [104] HILL K., GIOIA G. and TOTA V., *Phys. Rev. Lett.*, **91**, (2003) 064302.
- [105] SANDERS B.E. and ACKERMANN N.L., *J. Eng. Mech.*, **117**, (1991) 2396.
- [106] NOTT P. and JACKSON R., *J. Fluid Mech.*, **241**, (1992) 125.
- [107] FORTERRE Y. and POULIQUEN O., *Phys. Rev. Lett.*, **86**, (2001) 5886.
- [108] LUN C.K.K., SAVAGE S.B., JEFFREY D.J. and CHEPURNIY N., *J. Fluid Mech.*, **140**, (1983) 223.
- [109] LUN C.K.K., *J. Fluid Mech.*, **233**, (1991) 539.

- [110] LUDING S., HUTHMANN M., MCNAMARA S. and ZIPPELIUS A., *Phys. Rev. E*, **58**, (1998) 3416.
- [111] BIZON C., SHATTUCK M.D., SWIFT J.B. and SWINNEY H.L., *Phys. Rev. E*, **60**, (1999) 4340.
- [112] HILL K., JAIN N. and OTTINO J., *Physical Review E*, **64**, (2001) 011302.
- [113] WILLIAMS J.C., *Powder Techno.*, **15**, (1976) 245.
- [114] ROSATO A., STRANDBURG K.J., PRINZ F. and SWENDSEN R.H., *Phys. Rev. Lett.*, **58**, (1987) 1038.
- [115] METCALFE G. and SHATTUCK M., *Physica A*, **133**, (1996) 709.
- [116] FEITOSA K. and MENON N., *Phys. Rev. Lett.*, **88**, (2002) 198301.
- [117] ALAM M. and LUDING S., *J. Fluid Mech*, **476**, (2003) 69.
- [118] BAGNOLD R.A., *The Physics of Blown Sand and Desert Dunes* (Methuen and Co. Ltd., London) (1954).
- [119] DURAN J., *Phys. Rev. Lett.*, **84**, (2000) 5126.
- [120] VITTORI G. and BLONDEAUX P., *J. Fluid Mech.*, **218**, (1990) 19.
- [121] PAK H.K., VAN DOORN E. and BEHRINGER R.P., *Phys. Rev. Lett.*, **74**, (1995) 4643.